ECS The Electrochemical Society

OPEN ACCESS

Gold-coated Impedance Biosensors on PCB and PET for Real-Time Monitoring of Cancer Cells

To cite this article: Ahmad Fairuzabadi Mohd Mansor *et al* 2024 *ECS Sens. Plus* **3** 042401

View the article online for updates and enhancements.

You may also like

- Review—Challenges in Lab-to-Clinic Translation of 5th/6th Generation Intelligent Nanomaterial-enabled Biosensors
Rishi Kumar Talreja, Harsh Sable, Vikash Chaudhary et al.

- Review—Metal Oxide Chemoresistive Gas Sensing Mechanism, Parameters, and Applications
Abhilash Pathania, Neetu Dhanda, Ritesh Verma et al.

- Editors' Choice—Challenges and Opportunities for Developing Electrochemical Biosensors with Commercialization Potential in the Point-of-Care Diagnostics Market
Amir Ali Akhlaghi, Harmanjit Kaur, Bal Ram Adhikari et al.

ECS Sensors Plus, 2024 **3** 042401

Gold-coated Impedance Biosensors on PCB and PET for Real-Time Monitoring of Cancer Cells

Ahmad Fairuzabadi Mohd Mansor,[1] Salmah Sedek,[2] Anis Nurashikin Nordin,[1,z]
Muhammad Farhan Affendi Mohamad Yunos,[1] Zambri Samsudin,[3] Lai Ming Lim,[3]
Muhammad Irsyad Suhaimi,[4] and Lun Hao Tung[3]

[1]VLSI-MEMS Research Unit, Kulliyyah of Engineering, International Islamic University Malaysia (IIUM), Gombak, Malaysia
[2]Kulliyyah of Allied Health Science, International Islamic University Malaysia (IIUM), Kuantan, Malaysia
[3]Manufacturing Technology and Innovation (MTI), Jabil Circuit Sdn. Bhd., Penang, Malaysia
[4]Jabil Customer Solutions Center (JCSC), San Jose, California, United States of America

Electrical cell-substrate impedance sensing (ECIS) biosensors are widely used for in vitro cancer cell monitoring as they are label-free, require small sample volumes, and allow real-time monitoring. ECIS electrodes are typically made of pure gold, but the usage of pure gold electrodes is too costly for single-use applications. As an alternative, this work proposes the use of gold coatings on a printed sensor's electrodes. The interdigitated electrode design was used on glass fiber-reinforced epoxy resin for printed circuit boards (PCB), and polyethylene terephthalate (PET). The Cu/Ni electrodes on PCB were electroplated with Au, while the Cu/Ni electrodes on PET were coated with Au using an electroless technique. The physicochemical properties were studied using optical microscopy, scanning electron microscopy, and energy-dispersive spectroscopy. Electrochemical characterization was done using cyclic voltammetry and electrochemical impedance spectroscopy. Biocompatibility assessment and sensor functionality tests were done by culturing SiHa cervical cancer cell lines on these sensors and impedance measurements. The results show that both electroplated and electroless sensors were biocompatible and suitable to monitor SiHa cell growth. Electrochemical migration effect was observed on the sensors where the reaction occurred at 1.2 V DC for the PCB sensor and 1.0 V DC for the PET sensor.

Accurate monitoring of cellular growth in cell culture is crucial to provide information on cellular functions, processes, and behaviours. For cancer cells, *in-vitro* monitoring allow research on cancer biology, drug discovery, identification of therapeutic targets and personalized medicine to be conducted. In contrast, conventional cell-culture monitoring methods such as microscopic imaging, immunohistochemical staining, and flow cytometry perform end-point measurements and require expensive setup. Electric cell-substrate impedance sensing (ECIS) is seen as a viable cell sensor alternative as it enables stable, non-invasive, label-free, and continuous real-time read-out from the living cell monolayer. This technique utilizes a two-electrode setup consisting of a working electrode (WE) and a counter electrode (CE).[1,2] ECIS concept applies low alternating voltage to the cells via electrodes and measures their response,[3] enabling researchers to study the cell-cell and cell-substrate interactions. Seeded cells will adhere, spread, and proliferate on the electrode, forming an insulating layer. The insulation layer restricts the current movement between the electrodes, resulting in an increased impedance measurement, proportional to the number of cells attached to the electrode surface. The changes in impedance and phase response at specific frequencies provide valuable information related to the physical aspect of cell phenomena such as cell spreading,[4] wound healing,[5,6] cell signaling,[7] cell invasion,[8,9] and cell line classification.[10]

CV and EIS can be used for qualitative and quantitative of electrochemical sensing. They typically consist of a three-electrode setup of a working electrode (WE), a reference electrode (RE), and a counter electrode (CE).[11,12] In CV and EIS, a potential applied to the WE is swept back and forth for a defined number of cycles over a given range of voltage and speed of voltage sweep. As the potential is scanned across a specified potential range, the resulting current at the WE is measured.[11] While CV and EIS are valuable techniques for studying electrochemical reactions, they are not suitable for

assessment of physical aspect of cell behavior.[13] For example, CV requires applying a high voltage or current to the electrode, which can potentially damage cells or alter their behavior.[14] In this work, the biosensor and electrodes were designed specifically for ECIS application using two electrode system. Additional electrochemical characterization through CV and EIS was also performed.

The sensitivity of ECIS electrode depends on the design, material, and surface characteristics of the electrodes. Early ECIS designs include circular coplanar electrodes[2] which later were redesigned into interdigitated electrodes (IDE) in order to have larger effective sensing areas.[15] Gold (Au) is the preferred material for ECIS electrodes as it is inert, has high conductivities, and is biocompatible.[9] Fabrication of gold microelectrodes usually requires a cleanroom-based evaporation process that is costly, making it an unsuitable technique for disposable point-of-need sensors.

Screen printing[16] and 3D printing[17,18] are low-cost, competitive fabrication methods that are simple, rapid, scalable, and very popular for fabrication of less complex microelectronic circuits. For biosensing, an alternative to the use of fully gold electrodes is to use a combination of metals for the electrodes. This composite metal can be fabricated using lower-cost methods such as printed circuit technology. The Lab-on-PCB (LoP) is an example of this approach which integrates biological devices with printed circuit boards (PCB). LoP is less costly compared to cleanroom-based Lab-on-chip (LoC) technology which focuses on the integration of micro-sized circuits with microfluidic devices. In contrast, LoP uses mm-sized printed devices composed of layers of conducting metals (copper, silver, gold, lead, and tin) on FR4 fiberglass interwoven with epoxy resin substrate.[19,20] LoP has been useful in many biomedical applications such as molecular diagnosis,[21] DNA amplification,[22] electrophoresis,[23] and electrolyte detection.[24] An emerging application of LoPs is disposable electrochemical biosensors, where the devices are only exposed for a short time to biological substances.[25]

Other drawbacks of miniaturized devices that affect both LoP and integrated circuits due to high current/voltage densities are

zE-mail: anisnn@iium.edu.my

electromigration (EM) and electrochemical migration. EM occurs in a high current density or temperature areas that cause migration of the metal atoms.[26,27] Electrochemical migration occurs when two oppositely biased and closely spaced electrodes are exposed to an aqueous electrolyte causing a form of corrosion.[28,29]

Despite advancements in cell-based biosensors, there has not been much focus on the usage of LoP for long-term in vitro cell culture. Studies on LoP devices employed for long-term (more than 24 h) direct contact cell culture are limited perhaps due to copper and nickel are toxic to cells[30] and cell exposure to these materials should be limited. Multiple studies have demonstrated that the LoP is a low-cost and biocompatible with in vitro cell culture through various surface modifications of copper electrode, including surface finishing,[31] solder masking[32] and gold plating[33] of the electrodes. However, none of these studies investigated the possibility of electrochemical migration occurrence within their sensors. Additionally, the voltage and current amplitude used for impedance measurements were not specified in all of these works.[31–33] However, since the reported studies observed biocompatibility and no corrosion, it can be assumed that the applied voltage and current were not high enough to trigger electrochemical migration formation. To address this gap, evaluation of the susceptibility of LoP biosensors to EM and electrochemical migration was done to determine the operating range of the sensor and its reliability, especially on cell-based biosensor application. Performing an electrochemical migration study can prevent electrode corrosion, which could damage the sensor and induce toxic effects on the cells.

This work investigates printed metal composites with gold coatings for cell sensor electrodes. We focus on the physicochemical characterization and biocompatibility of these sensors, the aspects that are often overlooked by other researchers but crucial for successful cell-based applications. The biosensor in this work will be used to capture changes in growing cancer cell lines such as adherence, proliferation, morphological changes, or detachment of cells at the cell-substrate interface level using the ECIS method.[34] The same sensor IDE design was printed on two different substrates namely PCB and PET, which were used and compared. PCB sensor is fabricated of electrolytic/electroplated hard gold on FR4 fiberglass substrate, while PET sensor is fabricated of electroless nickel immersion gold (ENIG) on thermoplastic polymer polyethylene terephthalate (PET) which are common substrates used in the electronics industry.[20] Physicochemical characterization was done using an optical microscope, scanning electron microscopy (SEM), and X-ray energy dispersive spectrometer (EDS) to study the geometrical parameters and metallization thickness layer of the sensors. This work also includes experiments on the electrochemical migration effect and its activation voltages which is not commonly investigated in LoP devices. The biocompatibility and functionality of sensors were studied by culturing cancer cell lines on these sensors using SiHa cell lines as a relevant model for studying epithelial cells. The ECIS technique employed in this study is designed for adherent cell types, which are primarily categorized into epithelial-like or fibroblast-like morphologies. Observing the growth of cancer cells is crucial to provide real-time and specific insights into cellular responses, facilitating advancements in medical diagnostics, drug development, and personalized medicine.

Experimental

Methods.— *Electrode design.*—ECIS electrodes require a large effective surface area in order to accurately capture any changes in the cells. This can be best attained by implementing arrays of IDEs design.[3] Optimization of IDEs parameters was conducted by using COMSOL Multiphysics to simulate the electrical behavior of the electrodes in order to have low cut-off frequency, solution resistance, and the highest average electric field. The effect of varying geometrical parameters of electrode widths (W), spacing between electrodes (S), and total number of electrodes (W) was previously reported in.[35] For this work, the optimized IDEs parameters were

electrode length, $L = 7000\,\mu m$, the width-to-spacing ratio of 0.54 where width, $W = 295\,\mu m$, spacing, $S = 160\,\mu m$ and number of electrodes, $N = 18$. Despite thinner electrode width being associated with better sensitivities, this configuration could not be designed smaller due to the PCB fabrication limits.

Fabrication of PCB sensor.—In this work, array of IDEs were designed using Eagle software (Autodesk Inc.) with the following process specifications: 5 mils (127 μm) minimum metal trace width and 5 mils (127 μm) minimum spacing between traces. Fabrication was done by a commercial PCB manufacturer (HK Weiku Technology, Hong Kong) using a standard photolithography process on FR4 (flame retardant) glass fiber substrate. 1 oz of Cu ($\sim$35 μm) was selected as the Cu thickness of the PCB. The fabrication process is illustrated in (Fig. 1a). Since Cu can be toxic to cells, Cu was then covered with electrolytic Ni/Au and selected as the surface finishing of the sensor. The nickel (Ni) underlayer was electroplated on the Cu to provide mechanical support, diffusion barrier, and pore corrosion inhibitor for the Au surface. Au was then electroplated directly onto the Ni surface. To finish the sensor, an 8-well culture chamber (Thermo Fisher Scientific, USA) was glued to the sensor using a 10:1 ratio of polydimethylsiloxane, PDMS to curing agent (SYLGARD 184; Dow Inc., USA) and baked at 80 °C for 30 min. The final PCB sensor is shown in Fig. 1c.

Fabrication of PET sensor.—Fabrication and assembly of the PET sensor were done by Jabil Circuit. The same IDE sensor design was fabricated using an electroless plating method. The surface of the PET film was first treated and printed with silver IDEs patterns. Next, the PET film is immersed into a reducing agent containing a catalyst that allows metal ions (Cu) to deposit onto the silver patterns. The Cu traces were then coated with Ni and Au through another electroless plating and immersion process. After the IDEs were fabricated, the PET film was bonded onto a reinforced PET plate, to provide mechanical strength to the flexible sensor film and culture chamber on the top using a UV cure epoxy resin. UV curing epoxy was dispensed on the PET plate and sensor film, following the sequence of PET plate, sensor film then culture well and exposed to 365 nm wavelength UV light for 20 s to cure. The process is illustrated in (Fig. 1b). and the final PET sensor is shown in (Fig. 1d).

Physicochemical characterization.—The first test is the physicochemical characterization where the dimension, surface and composition of the electrode were analyzed using microscopic technique. The second test is the electrochemical migration test where the effect of electrode in direct contact with cell growth media solution and DC voltage bias.

Dimension and surface characterization.—Both the PCB and PET sensors' geometry and material thickness were analyzed using optical microscopy (Carl Zeiss Axio Lab.A1), scanning electron microscopy, SEM (JEOL, JSM-IT100), and energy-dispersive X-ray Spectroscopy, EDX (Oxford Instruments, AztecOne EDX). The electrodes were cut to 1 cm × 1 cm for the purpose of SEM imaging. The electrode surface and the cross section of the cut electrode were observed under the SEM with an accelerating voltage of 18.0 kV for electrode surface and 20.0 kV for electrode cross section. The contents of elemental spectra in the layers of sensor were determined using an EDX operated at 20 kV on the cross-sectional electrode image. Such elements of Cu, Ni, and Au in the sensor samples were determined using standard materials in the library.

Electrochemical migration test.—Electrochemical migration is defined as the growth of conductive metal filaments across a printed circuit board (PCB) in the presence of an electrolytic solution and a DC voltage bias.[36] In this work, the usage of thin metal lines ($<$10 μm) width as sensing electrodes makes them easily prone to the electrochemical migration effect. Since most biosensing

application involves the introduction of fluidic samples in contact with the electrodes, utilizing noble metals with higher standard electrode potentials (e.g. Au, Pt, and Ag) would eliminate the tendency of having an electrochemical migration effect.[28] Noble metals such as Au ($\sim$428 S m^{-1} conductivity) are expensive and have lower conductivities compared to Cu ($\sim$642 S m^{-1} conductivity). To counter this, printed circuit manufacturers prefer to utilize composite metals such as Cu/Ni/Au. Ni layer is placed in the middle to avoid diffusion of Cu into Au.[37]

The susceptibility of the sensor to electrochemical migration was tested by exposing both PET and PCB sensors to DMEM cell culture media with applied DC voltage. For this test, 500 μL of DMEM was pipetted into each biosensor well. Varying DC voltages were applied at the working electrode starting from 0 V to a maximum of 2.3 V with increments of 0.1 V every 5 min at room temperature. This experiment was conducted while observing the electrodes under a Dino-Lite portable microscope. Once electrochemical migration or burning marks were observed, the applied voltage ceased. The electrodes were rinsed with distilled water, dried, and observed under an optical microscope (Carl Zeiss Axio Lab.A1) for better image resolution.

Electrochemical characterization.—The PCB and PET sensor, consisting of a gold working electrode, a gold counter electrode and a silver wire reference electrode, were connected to an EmStat Pico Development Kit (PalmSens, Netherlands) and controlled with the PSTrace 5.10 interface software. The electrochemical performance of the test was evaluated by conducting cyclic voltammetry of 0.01 M [Fe(CN)$_6$]$^{3-}$ in 0.1 M KCl, between -1 V and 1 V at scan rates of 100 mV s^{-1}. Ep and I_p values were extracted using the software peak search function and the performance was compared against a DropSens screen-printed gold electrode. The electrochemical impedance spectroscopy was also conducted in 0.01 M [Fe(CN)$_6$]$^{3-}$ in 0.1 M KCl using EmStat Pico Development Kit controlled with the PSTrace 5.10 interface software. All the EIS experiments were carried out across a frequency range of 100 MHz-1 Hz with and AC voltage amplitude of 10 mV.

Biological characterization.—The second test is the biological test where the biocompatibility and sensor functionality were tested using SiHa cell lines. Biocompatibility test was done using microscopic observation of cell behaviour in contact with the electrode. Sensor functionality was done using impedance measurement of the cell growth compared to the conventional method of cell counting using trypan blue exclusion.

Sensor sterilization.—Sterilization is essential for any material used in cell culture to prevent contamination. Various methods exist,
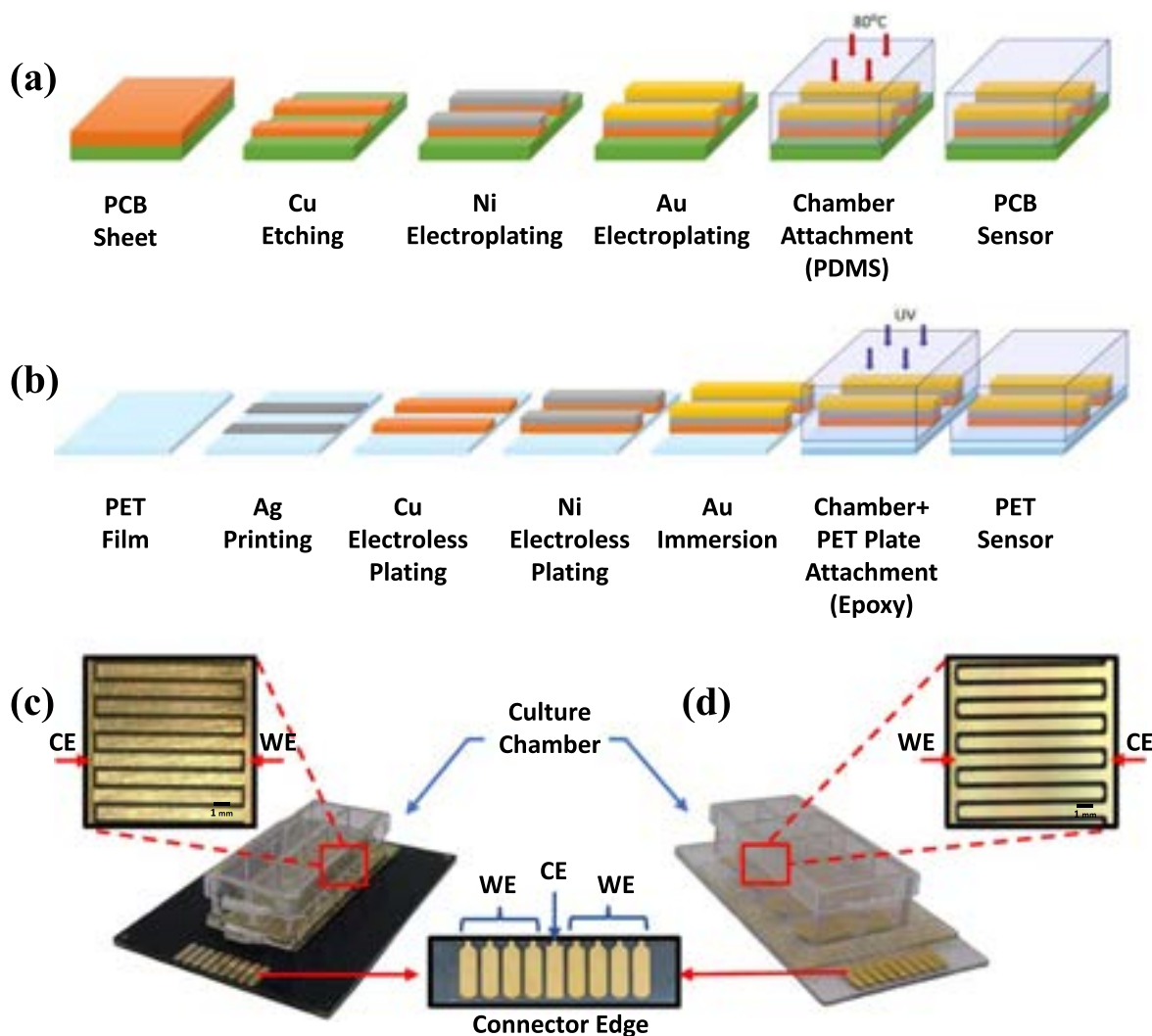

Figure 1. Workflow of the fabrication process (a) Fabrication process of PCB sensor based on photolithography, electroplating, and chamber PDMS attachment. (b) Fabrication process of PET sensor based on electroless plating, immersion, and chamber Epoxy attachment. (c) Oblique view of the PCB sensor with culture chamber. (d) Oblique view of the PET sensor with culture chamber. (Inset) Enlarged view of the IDEs configuration with the working electrode (WE) and counter electrode (CE) under an optical microscope at 4× magnification (scale bar is 1 mm).

including gamma radiation, ethylene oxide gas, UV light, and steam autoclave.[38] However, some methods are not suitable for the sensor in this study. Ethylene oxide gas and gamma irradiation, though effective, are not readily available in all labs. Steam autoclaving, a common practice for sterilizing cell culture consumables, is unsuitable for this work due to the heat-sensitive of PCB and PET sensor. Exposure to high temperatures (121 °C–148 °C) and humidity in a steam autoclave can damage the electrodes through corrosion, swelling, or cracking.[39] Corrosion arises from moisture, while swelling and cracking result from moisture absorption by the substrate and exposure to high temperatures. In this work, the sterilization was done using combination of UV sterilization and ethanol as there are no observable effect to the material properties.

The sensors were first cleaned using filtered water. This step removes any visible dirt, debris, or contaminants from the surface of the sensors. After cleaning, the sensors were sterilized by immersing them in a 70% ethanol solution (HmbG, Malaysia) in an ultrasonic bath during this process. The frequency waves create cavitation bubbles that helps to remove any remaining contaminants and ensures a thorough cleaning of the sensor surfaces. After sterilization with ethanol, the sensors were rinsed using phosphate-buffered saline (PBS; Nacalai Tesque, Japan). This step removes any residual ethanol from the sensor surfaces, ensuring that it does not interfere with subsequent experiments or analyses. Finally, the sensors were sterilized under UV light in biosafety cabinet for at least 2 h in a biosafety cabinet. UV light is a powerful sterilizing agent that can effectively kill microorganisms by damaging their DNA or RNA.

Biocompatibility tests.—Two different biological characterization experiments were conducted using the sensor namely, biocompatibility of sensor material and cell growth monitoring. The International Organization for Standardization (ISO) prioritizes quantitative methods (e.g., MTT/XTT) for biocompatibility assessment, as outlined in the ISO 10993 series of standards and the USFDA's guidance on ISO 10993–1.[40] The materials used in this study have been reported to be biocompatible through quantitative assessment according to the ISO standard. For example, previous in vitro studies using MTT assay on PET plastic particles[41] and cytotoxicity assays on PCB FR4 substrates[32,33] have demonstrated their non-toxicity to cell cultures. Stock et al. in their work studied the effect of microplastics particle materials such as polyethylene (PE), polypropylene (PP), polyethylene terephthalate (PET) and polyvinyl chloride (PVC) on human cell lines Caco-2, HepG2 and HepaRG.[41] The cytotoxicity tests were conducted using MTT assay in 96-well plates. Based on the results, the percentage of cell viability for PET is greater than 80% for all type of cell lines. The work concluded that PET particles do not trigger acute toxic effects, regardless of the shape and material. On the other hand, biocompatibility of PCB material was also shown in different studies. Urbano-Gámez et al. in the work studied the biocompatibility of PCB on mouse retinal explants cell culture.[23] The cells were cultured in PCB-PMMA and MEA-resin closed loop systems. At the end of experiment, the tissue was disaggregated before staining, dead cells were labeled with 2-(4-amidinophenyl)-1H-indole-6-carboxamidine (DAPI; 1:2500 in cytometry buffer) and measured by flow cytometry. The results show that PCB with solder mask preserved retinal cell viability similar to the control environment thus indicating the biocompatibility of the material. In other work, Rabbani et al. have also studied the biocompatibility of PCB material with human dermal fibroblasts. The biocompatibility was tested using 24-well plates where the electrode was exposed to the cell culture and live-cell count was done after 48 h of exposure. The findings show that no evidence of corrosion or adverse effect on the cells was observed. They concluded that the proposed PCB electrodes provide good biocompatibility for in vitro cell cultures.

Therefore, this work employed a simple qualitative direct contact approach for biocompatibility testing, where the sensor material was directly exposed to cells in suspension for 48 h within a T-flask. The sample material is considered non-toxic or minimally toxic if it does not cause any irregularity in the cells. Observable changes in the cell include changes in morphology and cell growth that repel away from the sample. In this experiment, both sensors were cut into 1 cm × 1 cm squares at the IDEs electrodes. This is to ensure that all metal layers and the substrate were exposed to cells and the culture medium. Prior to cell exposure, the samples were sterilized under UV light for 2 h. The samples were immersed in the growth media together with SiHa suspension cells in the T-Flask. The samples were placed in the middle of the T25 flask to avoid any light refraction during imaging. The experimental setup is illustrated in (Fig. 2b). The images were taken and analyzed after 24 h and 48 h of sample exposure to the cells.

Cell growth impedance measurements.—The second part of the test is impedance cell growth monitoring. In this test, cells were directly cultured on the electrode inside the culture chamber, and cell growth was observed via measurements of cell impedance. Prior to cell culture, the sensor was coated with an extracellular matrix (ECM). Gelatin solution (Sigma-Aldrich, Germany) was used as the ECM for the sensor. Each electrode surface was coated with approximately 100 μl of gelatin per well. Gelatin was allowed to dry for at least 2 h in the biosafety cabinet before the cell medium was introduced onto the sensor. Next, each sensor well was seeded with 500 μl cell suspension at a cell density of 1×10^5 cells ml^{-1}. The inoculated sensors were left in the biosafety cabinet at room temperature for 30 min for the cells to settle uniformly over the electrodes and to avoid the thermal convection effect once placed in the incubator. The cells were then placed in the incubator (LabServ, Thermofisher) for 96 h.

The impedance measurements were performed by applying AC signals with a peak-to-peak amplitude of 500 mV using a precision LCR meter (Good Will Instrument Co.) at a frequency of 1 kHz. In this work, a 500 mV peak-to-peak amplitude was selected as it is generally low enough to avoid inducing significant stress or damage to the cells, while still providing a strong enough signal for reliable impedance detection. Higher amplitudes could potentially alter cell behavior or even cause cell damage triggering cell apoptosis.[42,43] For frequency selection, our previous studies on impedance spectroscopy of cells had been conducted using frequencies ranging from 40 Hz to 10 MHz.[44,45] These studies found that a low frequency of 1 kHz was optimal and effective for measuring cell impedance. This is due to at lower frequencies, impedance measurements are more sensitive to changes in the cell-substrate interface and cell morphology.[43] For bioimpedance studies, the alpha (α) dispersion region (~10 Hz to 10 kHz) can provide information on tissue structure and composition[46] thus providing insights into cell adhesion and proliferation. The single-frequency method has proven to be an effective and is an adopted technique in commercialized devices such as ECIS device[47] and xCELLigence.[48] Therefore, in this work, a single frequency of 1 kHz was selected for the impedance measurements rather than a full impedance spectrum.

Impedance responses were taken every 24 h for a total of 96 h. The impedance measurements were later converted to cell index (CI) values for a better representation of the cellular behavior. The cell index was calculated based on the following Eq. 1:[49]

$$Cell\ Index\ (CI) = \frac{|Z_t| - |Z_0|}{|Z_0|} \quad [1]$$

Where,

$|Z_t|$ = Impedance of the chamber with cells at specific time t.

$Z_0|$ = Impedance of the chamber without cells at time 0.

As CI is a function of impedance values, it provides quantitative insights into the biological behavior of the cells, including cell number, viability, and morphology. The magnitude of the CI is higher when more cells are attached to the electrodes under the same physiological conditions. For example, if cells undergo morphological changes such as elongation, retraction, or clustering, these alterations will be reflected in the CI based on the cell-substrate
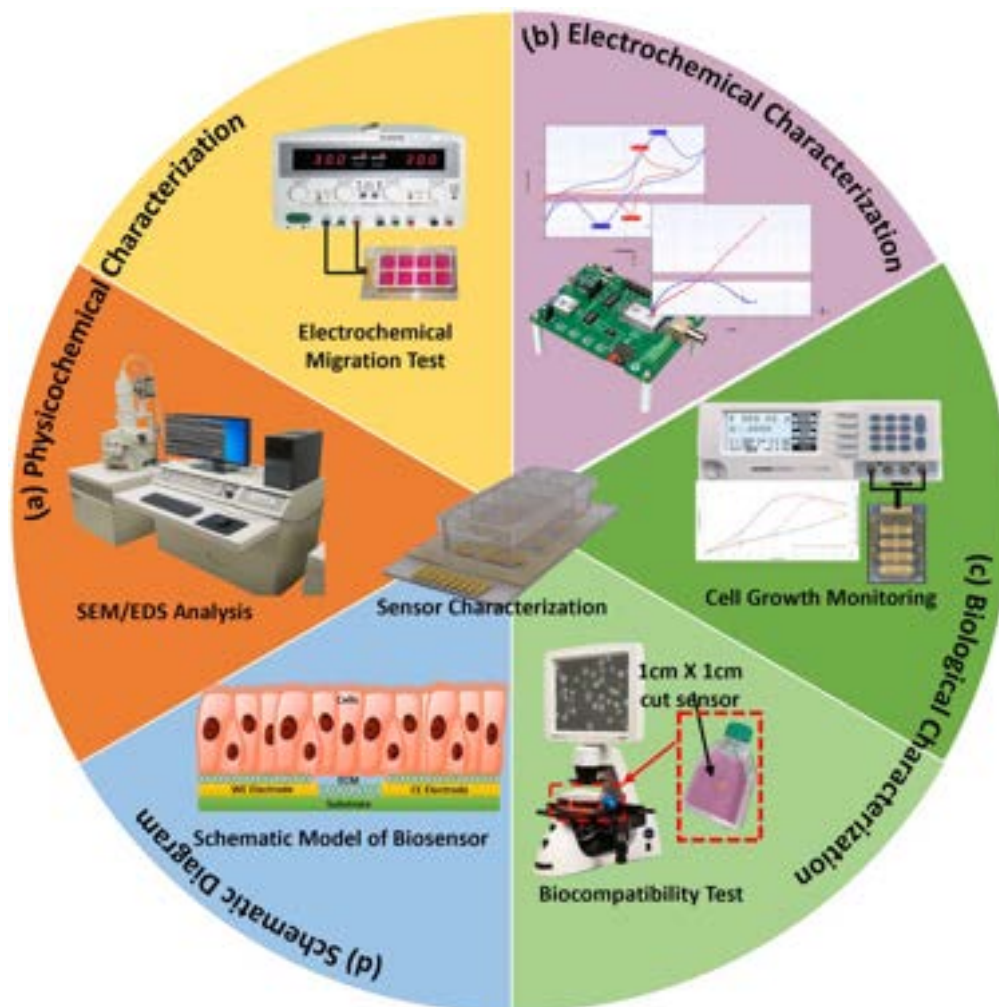
Figure 2. Schematic illustration of the experimental setup for sensor characterization. (a) Physicochemical characterization comprised of SEM/EDS analysis and electrochemical migration test. (b) Electrochemical characterization which includes CV and EIS measurements (c) Biological characterization consists of biocompatibility test and cell growth monitoring. (d) Schematic illustration of the cell-electrode model in the biosensor.

interaction.[50] Increase in CI could also be due to the adhesion strength of cell-electrode and cell-cell interaction.[50] In contrast to cell index values, cell number is only related to the population of cells and is measured in the trypan blue method by loading the sample into the hemocytometer chamber and counting the number of cells on the grid under the microscope. CI can be considered as a more comprehensive value compared to just cell number.

All measurements were done in triplicates. Microscopic images of cells on electrodes were taken at 96 h using an inverted microscope (Evos XL Core) for the PET sensor and an upright microscope (Carl Zeiss Axio Lab.A1) for the PCB sensor with the opaque substrate. The schematic illustration of the cell-electrode model inside the biosensor is shown in (Fig. 2c).

Results and Discussion

Selection of materials.— *PCB sensor.*—Printed circuit board or PCB is the standard industrial method for making electronic circuits. It starts as a sheet of insulating glass fiber-reinforced epoxy resin as substrate, with a layer of copper (Cu) as a conductor on one side. The pattern of conducting tracks and pads is printed or photolithographed onto the Cu to make the circuit connections. To avoid Cu oxidation and to provide a solderable surface, most PCBs have different surface finishes to maintain their performance. Surface finishes are essential for making a reliable PCB board while strictly complying with the Restriction of Hazardous Substances (RoHS).

Some examples of surface finishes include immersion silver, electroless nickel immersion gold (ENIG), Electroless Nickel Electroless Palladium Immersion Gold (ENEPIG), and Electrolytic Nickel/Gold (Hard Gold). By exploring the low fabrication cost and widely available commercial PCB industry, this technique has the potential to produce sensors, especially in large-scale volumes.[24]

PET sensor.—PCB sensors have a cost advantage compared to PET sensors, as it is a commercial electronics fabrication process that has been optimized by the manufacturer. PCB biosensors, however, have a disadvantage as it has an opaque FR4 fiberglass substrate, which cannot be used with an inverted microscope. This feature is important in biosensors to observe the cells' structure or morphology during the growth or response after treatment. Transparent PET sensors on the other hand allow optical observation of cells on the electrodes.[51] PET is a common substrate for biosensors due to its biocompatibility and compatibility with optical techniques[20,21]. Conductive electrodes can be placed on top of PET using either electroplating or electroless methods. In this work, Cu was electroplated on a thin layer of silver followed by deposition of Ni and Au using the electroless process. All materials used for this PET sensor were prepared by JABIL Circuits.

The selection of the UV cure epoxy is crucial in order to ensure the reliability of the sensor during long-term cell culture. For this work, only thixotropic epoxy was selected. Thixotropy is the property of fluids and gels becoming thinner when applied with a

constant force, and the viscosity of the materials will recover to the initial state once the force applied is lifted.[52] An ideal epoxy for this application must be highly thixotropic so that after the UV cure epoxy is dispensed it will not flow away from the dispensed position. This epoxy will also remain constant and not seep through after dispensing when there is no external force. This allows the width and height of the dispensed bead line to be controlled well. The thixotropic properties and the recovery times of the UV cure epoxy were investigated by dispensing the epoxy onto the sensor film and leaving it for hours. Based on the assessment, the UV cure epoxy does not show a "seep" behavior, but a highly thixotropic behavior. It is essential to determine the recovery time of the epoxy so that spillage or overflow of epoxy can be prevented when the chamber is well attached to the sensor film with the dispensed epoxy.[53] Two different characterization tests were performed on the sensor to test its reliability and functionality as shown in (Fig. 2).

Physicochemical characterization of sensors.—Physicochemical characterization of the sensors was carried out to investigate the difference between the two types of Au-coated sensors on PCB and PET. Both sensors were sent for fabrication following the standard process from the respective manufacturer. The dimension of the whole board is 7 cm × 5 cm, as shown in (Fig. 3a). Each board comprises eight independent sensors and culture well with a common counter electrode (CE). The average measured dimension of one electrode finger of the PCB sensor is 309.8 ± 1.2 μm width and 139.8 ± 3.5 μm spacing while for the PET sensor is 298 ± 6.3 μm width and 148.6 ± 5.1 μm spacing as shown in (Figs. 3b and 3c). In terms of fabrication finish, the PCB sensor exhibits better straight edges

compared to the PET sensor with curvy edges. This shows that the electroplating process in PCB produces good electrode edges but slightly increases the width traces after Ni and Au coating on the Cu as can be seen in (Fig. 3d).

The electrode comprises of three different metal layers: Cu, Ni, and Au. Observation using an optical microscope shown in (Figs. 3d and 3e) illustrates that the overall thickness of the electrode in the PCB sensor is 43.5 μm and 5.6 μm for the PET sensor. Slight color changes can be observed for the different existing metal layers of Cu, Ni, and Au. Further analyses were done using SEM and EDX to analyze the surface and to verify the presence of these three materials as shown in (Fig. 4).

The SEM image shows that the electroplated PCB sensor in (Fig. 4ai) has smooth but wavy surface features while the electroless PET sensor in (Fig. 4bi) has fine grainy surface features. These surface morphologies have a major role in influencing the ECM coating and modulating cellular behavior such as adhesion, proliferation, and orientation.[54] Cross-sectional views of the sensors in (Figs. 4aii and 4bii) show more accurate measurements of electrode thickness as 45.7 ± 0.92 μm for PCB and 5.08 ± 0.04 μm PET sensor respectively. To analyze the elemental composition of the electrodes, EDX measurements attached to SEM were performed. The strong Cu peaks followed by Ni peaks and weak Au peaks shown in the spectrum and elemental mapping in (Figs. 4c and 4f) indicate the formation of Cu/Ni/Au layers with a percentage ratio of 84/9.7/6.3 for PCB sensor and 73.9/16.9/9.2 for PET sensor. Additionally, these ratios are further calculated into the thickness of each metallization layer approximately 37.6 μm/4.3 μm/2.8 μm for the PCB sensor and 3.7 μm/0.9 μm/0.4 μm for the PET sensor.
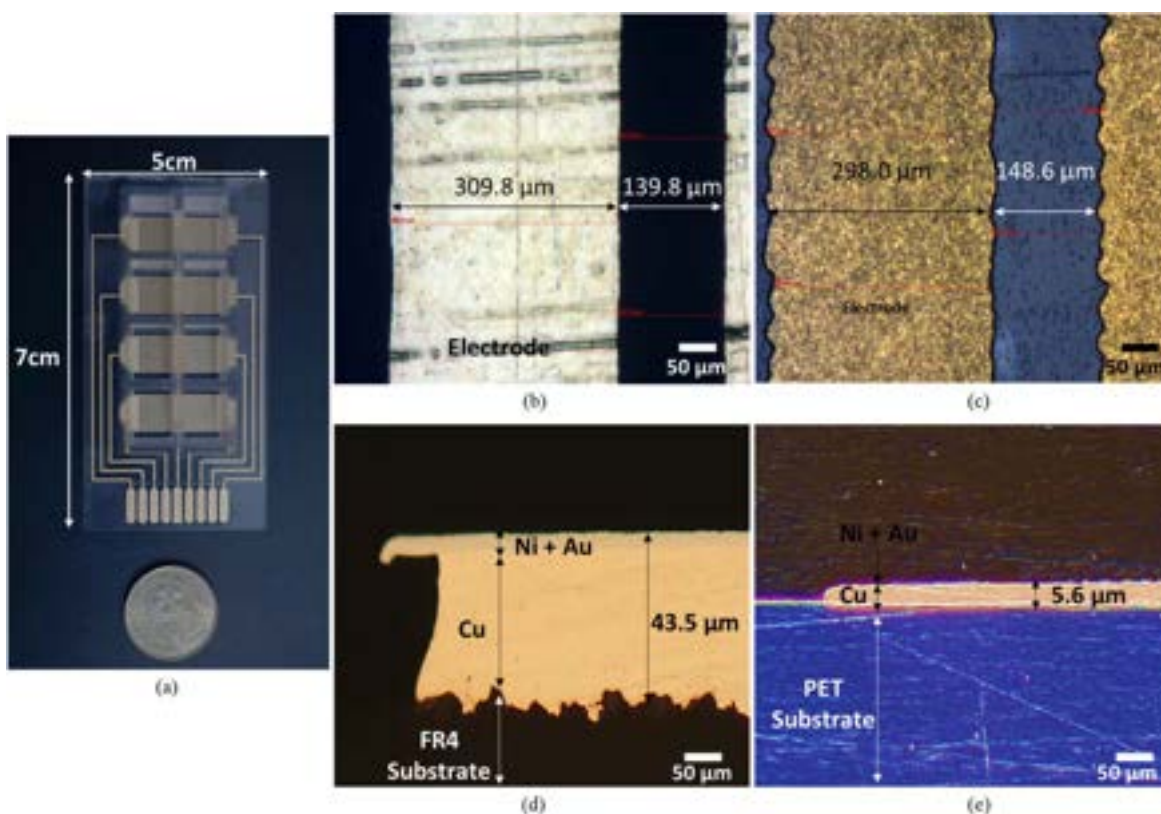

Figure 3. Characterization of electrodes dimension. (a) Dimension of sensor design. The image shown is for the PET sensor. PCB sensor has the same dimension of electrode configuration but a slightly larger substrate size (b) Micrograph image of a single PCB electrode finger at 10× magnification. The measured dimension of one electrode finger is 309.8 ± 1.2 μm width (n = 4) and 139.8 ± 3.5 μm spacing (n = 4). (c) Micrograph image of single PET electrode finger at 10× magnification. The measured dimension of one electrode finger is 298 ± 6.3 μm width (n = 4) and 148.6 ± 5.1 μm spacing (n = 4). (d) Cross-sectional image of PCB electrode at 2000× magnification. Different Cu and Ni layers could be observed from the color contrast between the two metals. (e) Cross-sectional image of PET electrode at 2000× magnification. Different Cu and Ni layers could be observed from the color contrast between the two metals. Images have been digitally enhanced (color saturation 200%) to aid visualization. All the microscopic images are in the scale bars of 50 μm range.
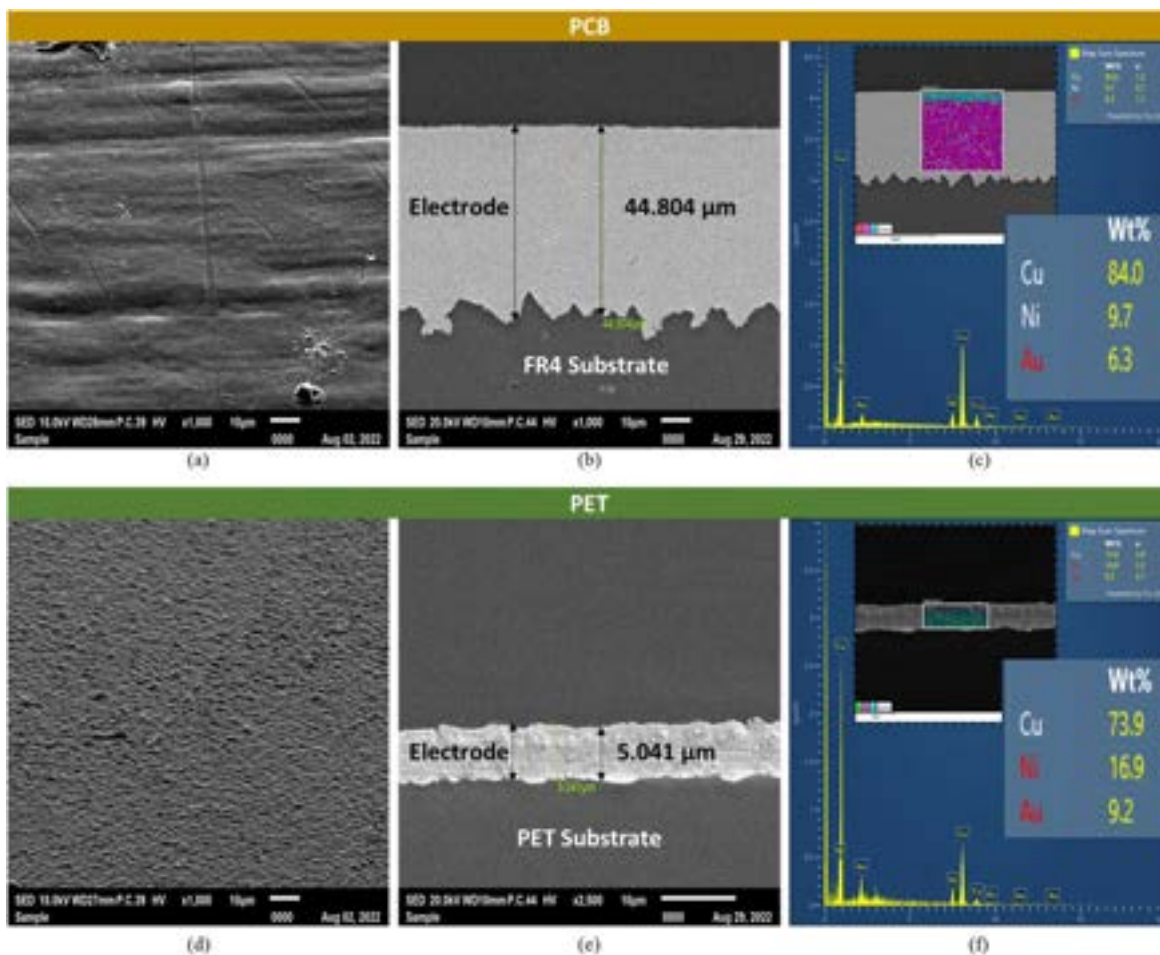
Figure 4. Characterization of electrode surface and thickness using SEM and EDX. (a) Morphological of the PCB sensor electrode surface. (b) Cross-sectional electrode of PCB sensor with a measured thickness of 45.7 ± 0.92 μm (n = 3). (c) EDX spectrum and elemental mapping of Cu, Ni, and Au in the PCB sensor. (d) Morphological of the PET sensor electrode surface (e) Cross-sectional electrode of PET sensor with measured thickness of 5.08 ± 0.04 μm (n = 3) (f) EDX spectrum and elemental mapping of Cu, Ni, and Au for PET.

Electrochemical migration effect.—Most of the biosensor's performance degradation can be attributed to the gradual deterioration of coating or sensing layer on the electrodes, which limits the sensor's shelf-life to several months under optimal storage conditions.[55,56] Consequently, disposable biosensors typically require usage within six months of fabrication.[57] In our work, the sensors' shelf-life is longer since the ECM coating is only done before the cell culture process. Therefore, degradation of the surface coating is only due to environmental factors such as temperature, humidity and light.[58] The electrode materials, namely PCB and PET are common materials used in printed electronics[59] and its long-term stability and environmental effect have been previously reported in.[60–62] Electroplated and electroless plated gold have shown good integrity and adhesion between the metallic layer and substrate and have low risk of delamination under standard operational conditions (e.g. room temperature, low humidity and no exposure to chemical solution). However, prolonged exposure of the sensor to moisture or liquid can weaken the bonds over time and with external voltage applied, could lead to oxidation of the copper and compromising the stability of the electrodes.[63] To summarize, gold-coated circuit board is robust, does not corrode or tarnish, and is only susceptible to the electrochemical migration due to the presence of water drops (WD) and temperature and humidity (THB) bias.[63] In this work, electrochemical migration was performed, specifically tested with the condition relevance to cell-based biosensor applications.

Figures. 5ai and 5bi shows the initial images of the electrodes with zero applied voltage. Electrochemical migration (ECM) causes tree-like growth of metal filaments that may result in short circuits. When high current densities flow into these dendrites, they may burn due to high heat dissipation.[36] This burning effect was observed during our experiments involving varying applied DC voltages to the sensors. The applied voltage bias creates an electric field that drives ionic migration and causes the positive ions to travel along the field lines from the anode to the cathode through an ion transport path provided by the aqueous medium.[36] For the PCB sensor, electrochemical migration starts to occur after 5 min with 1.2 V voltage bias, where burning marks were observed at the electrodes' edges as shown in (Fig. 5aii). Electrochemical migration occurs slightly earlier for PET sensors, where reduction can be seen at 1.0 V applied voltage (Fig. 5bii).

Previous research has indicated that there is a critical voltage bias range in which surface ECM occurs.[64] The minimum value of the critical voltage should be higher than the electrochemical potential values of each metal such as 0.13 V for tin/lead solder, 0.25 V for nickel, 0.34 V for copper, 0.8 V for silver, and 1.5 V for gold.[36] In this work, it was observed that the minimum ECM critical voltage value for PCB = 1.2 V and PET = 1.0 V. This is because the thickness of the Au layers was different; namely 2.8 μm for the PCB sensor and 0.4 μm for PET sensor. When voltage is increased, both burning and bubble generation occurred at 2.3 V for the PCB sensor (Fig. 5aiii) and 2.0 V for the PET sensor (Fig. 5biii). The presence of dendritic growth was also observed as white precipitation in both sensors using a high-resolution microscope as shown in (Figs. 5aiv and 5biv). The green precipitation in these figures is CuOH as previously reported by Medgyes.[29]
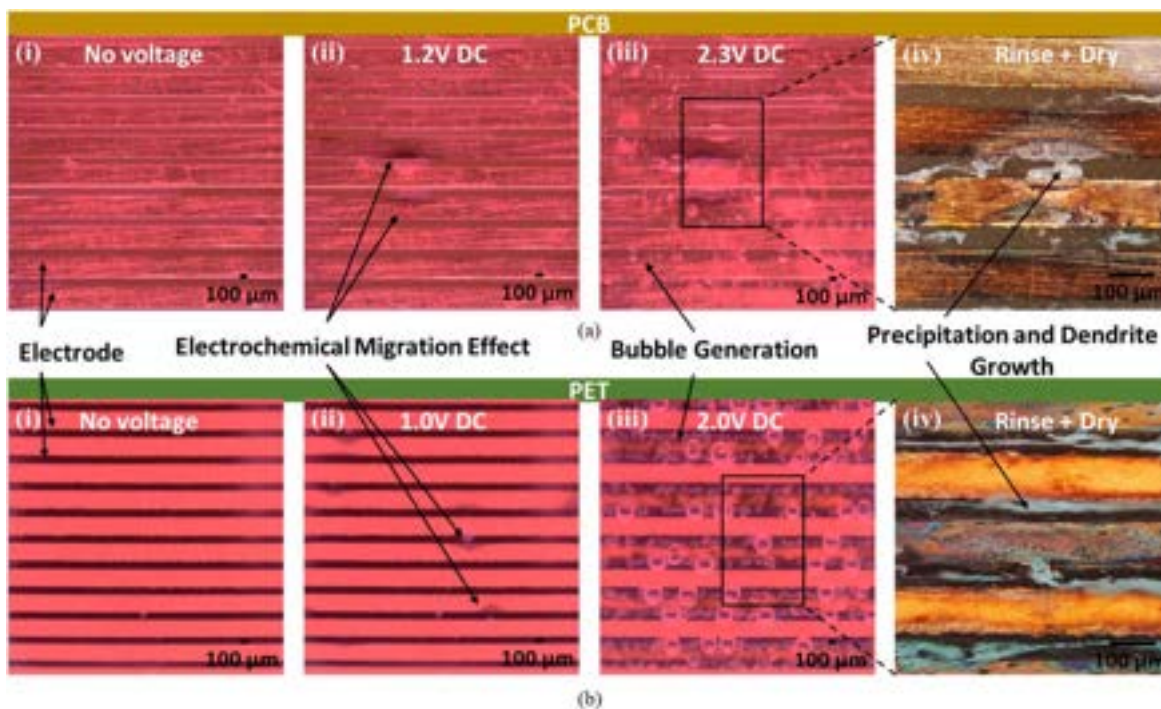
Figure 5. Electrochemical migration test in for the sensors immersed DMEM. (a) (i) The PCB sensor at 0 V. (ii) Effects of electrochemical migration was observed at 1.2 V bias voltage after 5 min of exposure. (iii) Instantaneous reaction and bubbling can be seen at 2.3 V (iv) Optical image of the sensor using high resolution microscope Carl Zeiss Axio. (b) (i) PET sensor at 0 V bias. (ii) Electrochemical migration effect at 1.0 V bias voltage after 5 min of exposure. (ii) Instantaneous reaction and bubbling can be seen at 2.0 V bias voltage. Both electrochemical migration effects left Cu precipitate and dendrite growth after the rinsing and drying process(iv) Optical image of the sensor using high resolution microscope Carl Zeiss Axio. All scale bars for the microscopic images are in 100 μm range.

Several factors may influence the rate of ECM including temperature, relative humidity, voltage bias, conductor material, conductor spacing, contamination type, and contamination amount.[36] ENIG tends to be more resistant to ECM due to the nobility of the gold. The top Au layer protects the Ni and Cu layers underneath. Any defects that occur in the Au plating would expose the more reactive Ni layer, making it more susceptible to migration.[28]

Electrochemical performance.—The electrochemical performance of the PET and PCB sensors was characterized by cyclic voltammetry and electrical impedance spectroscopy (0.01 M ferricyanide in 0.1 M KCl solution). Figure 6a compare the cyclic voltammogram of the PET and PCB sensors with a commercial DropSens screen-printed gold electrode (SPGE). The peak currents recorded for the PCB, PET, and SPGE sensors were 0.493 mA, 0.326 mA, and 0.224 mA, respectively. Both PCB and PET sensors exhibited higher peak currents compared to the SPGE, indicating better detection of electroactive ions in the ferricyanide solution. This is potentially attributed to the larger effective electrode surface area of the PET and PCB sensors compared to the SPGE, as expected by the Randles-Sevcik equation.[65] With a larger surface area, the diffusion of electroactive species to the electrode surface is improved, which can enhance the overall current response from the sensor.

The peak current separation ΔE_p, of the sensor was found to be 103 mV for PET sensor and 253 mV for PCB sensor both larger value than that of SPGE, 79 mV. This shows that PET sensor exhibits better performance than PCB sensor by having low barrier to electron transfer[66] (better reversibility) as indicated by the smaller ΔE_p. The peak current separation and oxidation–reduction peak ratio of for PET sensor ($Ipa/Ipc = 1.093$) implies good reversibility of the ferri-/ferrocyanide cycling on the device, although the value is slightly higher than the ideal reversible system ($Ipa/Ipc = 1$) compared to that of SPGE ($Ipa/Ipc = 0.941$). PCB sensor shows

oxidation–reduction peak ratio of ($Ipa/Ipc = 0.89$) but since the peak separation ΔE_p is large, it can be inferred that the reaction is considered as quasi-reversible.[67] Despite both the PET and PCB have lower performance than the commercial SPGE, the PET sensor peak separation is still comparable to other gold-based electrodes sensor with the peak fall within the range of 80 to 130 mV.[68–70]

Figure 6b compares the electrical impedance spectroscopy of the PET and PCB sensors with a commercial DropSens screen-printed gold electrode (SPGE) in 0.01 M ferricyanide. The PET sensor and SPGE produce a small semicircle in the Nyquist plot while the PCB sensor produces a wide semicircle plot. The inset of Fig. 6b shows the equivalent circuit used for fitting the response based on Randles model. Table I shows the fitted values for each parameter of a solution resistance (R_s), a charge transfer resistance (R_{ct}), a double layer capacitance (C_{dl}), and a Warburg impedance (Z_W). Both of PET and PCB sensors have low R_s which shows that the sensors have high conductivity and reduced ohmic loss[12] as compared to the SPGE. As previously mentioned, this is due to the larger effective electrode surface area of the PET and PCB sensors compared to the SPGE. This increased area allows better ion transport, therefore reducing the overall resistance in the solution. The IDEs create a more uniform electric field and allowing more active sites for electrochemical reactions, leading to lower solution resistance.[65]

PET has the lowest R_{ct} of 177.7 Ω indicating that the electron transfer between the electrode and the redox species is more efficient for this sensor. The low R_{ct} value supports the previous CV results of lower ΔE_p for PET sensor and SPGE compared to PCB sensor.

Similar to previous discussion on electrochemical migration, the electrochemical testing has shown that the measurements are causing destructive effects on the sensor. Despite the low voltage applied (-1.0 V to 1.0 V) in CV and (10 mV) in EIS, the formation of dendrite can still be seen in both sensors after the CV and EIS sweep as shown in Figs. 6c and 6d. This is due to the high presence of chloride ions in the buffer solution of potassium chloride, KCl. The presence of chloride ions could lead to the faster corrosion of Au and
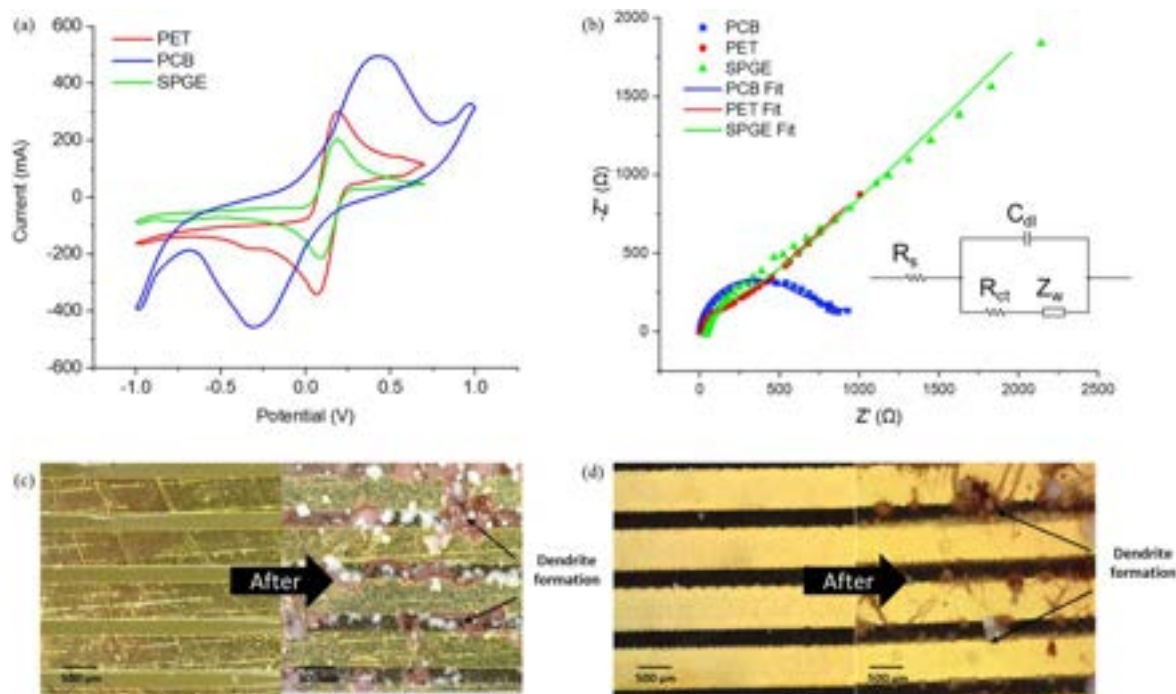
Figure 6. Electrochemical characterization of PET and PCB sensors (a) Cyclic voltammogram comparison of PET and PCB sensors vs commercial DropSens SPGE in 0.1 M potassium ferricyanide in 0.01 M KCl solution at 100 mV s^{-1}. (b) Electrochemical impedance spectroscopy of PET and PCB sensors vs commercial DropSens SPGE in 0.1 M potassium ferricyanide in 0.1 M KCl solution at ac potential of 10 mV, frequency range 100 MHz to 1 Hz. Inset shows the Randles equivalent circuit fitting of the model. (c) Precipitation and dendrite formation on PCB sensor after the electrochemical characterization (d) Precipitation and dendrite formation on PET sensor after the electrochemical characterization. All the microscopic images are in the scale bars of 500 μm range.

Table I. The Randles equivalent circuit components and values extracted from EIS measurements. Fitting, percentage error and chi-squared value were all obtained from PSTrace software.

Sensor	R_s (Ω)	Error%	R_{ct}(Ω)	Error%	C_{dl}(μF)	Error%	Z_w(kσ)	Error%	Chi-Squared
PET	5.59	2.38	177.70	9.13	6.01	2.82	1.97	11.74	0.0177
PCB	2.01	8.40	614.50	7.09	4.73	4.15	0.79	5.19	0.0412
SPGE	58.40	2.45	232.80	13.26	4.27	6.42	4.83	4.19	0.0116

Cu interface based on study by Evans et. al.[71] Therefore, both sensors are unsuitable for reusable electrochemical applications despite the thickness of the plated gold in PCB sensor have shown to be up to 45 μm. The effect of the thickness of the plated gold in developing a reliable biosensing electrodes for Au-Ni-Cu has open to be explored for PCB-based biosensors.[25]

Biological characterization of sensor.—Another important aspect of sensor characterization is material cytotoxicity. A qualitative test was performed by introducing the sensors directly in contact with SiHa cells and growth media in T-Flasks for 48 h. The cells were examined under the microscope for any damage to cell morphology or unusual response in comparison to the control group. The images were taken using different magnifications due to the light refraction caused by the PET material causing the cells to be less visible at 10× magnification. Presence of any cytotoxic compound within the sensor would cause the cells to be either damaged, migrate away from the material, or induce cell death. The study from triplicate test inferred that both sensors are cell-compatible without any observable changes in cell morphology for 48 h compared to the control group as shown in (Figs. 7a–7c) respectively. Higher magnification images indicating cell growth on both PCB and PET is also shown in Fig. S2 of the supplementary material. Insertion of both sensor materials did not affect cell epithelial morphology.

However, it is worth noting that the number of cells visible near the edges of both (PET and PCB) within the T-flask were less

compared to the control. Reduction of the number of cells at the edges was also observed for both the PET and PCB test sensors inside the T-Flask. From the microscopic imaging, the less cell density near the edges of the PET and PCB sensors were likely due to the cells exhibiting adaptive behaviors in response to the mechanical stress.[72] When cells encounter new materials, such as in this case PET and PCB, the material properties and surface characteristics influence the adhesion and proliferation experienced by the cells.[73] The presence of the cut sensor inside the flask creates localized areas of mechanical stress on the cells near the edges.[74] The mechanical stress induced can disturb the cell-substrate adhesion and reduce the cell number and focal adhesion contacts between the cells and the culture substrate.[74] Due to this disruption in the mechanically stressed area, the cells cannot maintain strong adherence to the cell substrate leading to less cell density.[75] Presence of mechanical stress exerted on the cells could be quantified using the traction force microscopy technique.[76,86] This analysis was not included in the present work as there were still adherent and proliferation of cells near the sensor's edge, with no signs of migration away from the electrode; the materials are considered as biocompatible but are expected to exhibit a prolonged lag phase due to this adaptive cell behavior.

Sensor cell growth impedance measurements.—To verify that the sensors can be used to measure cell growth, SiHa cells were seeded and cultured in the cell culture chambers of both the PCB and
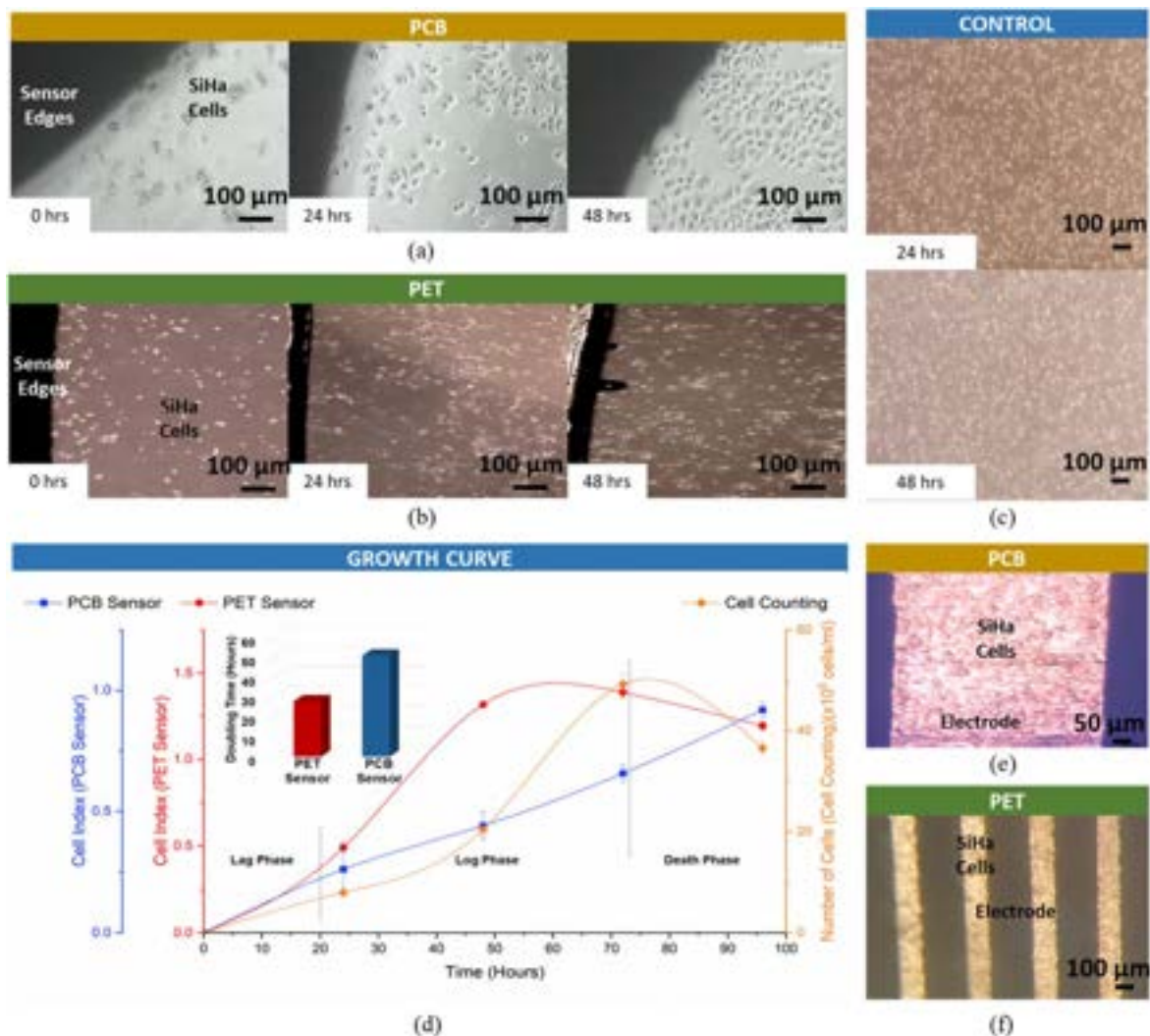
Figure 7. Cytotoxicity and cell growth monitoring on the sensors (a) Time interval image (10× magnification) of cut PCB sensor with direct contact with SiHa cells in T-Flask (b) Time interval image of cut PET sensor with direct contact with SiHa cells in T-Flask (c) Control cell growth in separate T-flask without sensor (d) Growth curves of SiHa cells cultured on both PET and PCB sensors in comparison with the conventional method of cell counting using trypan blue exclusion. The results are the mean cell index for 3 replicates ± SD. (Inset) Doubling time of SiHa cells in PET and PCB sensor. (e) Cell growth can be seen on the electrode in the PCB sensor observed under an upright microscope (opaque substrate) at 96 h. (f) Cell growth can be seen on the electrode in the PET sensor observed under an inverted microscope (transparent substrate) at 96 h. All the microscopic images are in the scale bars of 100 μm range except in figure (e).

PET sensors. The impedance measurements were acquired every 24 h for 96 h and converted to the cell index for a better representation of the cells. The cell growth curve is shown in (Fig. 7d). The growth curve using the trypan blue exclusion method and measured using the hemocytometer shows that the cells were proliferating and reached confluency at approximately 72 h before entering the death phase. The number of cells was seen to double every 24 h suggesting that the doubling time of the cells was approximately 24 h.

During the first 24 h, impedance measurements revealed an increase in cell index values for both sensors, indicating successful cell attachment to the gelatin ECM on the electrode surfaces.[77] This finding aligns with the cell counting growth curve (shown in Fig. 7d), where the lag phase suggests that cells are adapting to the new environment and synthesizing enzymes and factors needed for cell division,[78] explaining the slow initial growth. However, since the cells adhere to the gelatin-coated area, variations in gelatin coating efficiency can influence impedance measurements. Studies have shown that the yield and effectiveness of gelatin coatings depend on the substrate material and its surface properties.[79] Therefore, the higher cell index observed with the PET sensor compared to the PCB sensor suggests a potentially better yield of gelatin on the PET substrate.

The CI increase continues for both sensors between 24 to 48 h. The PET sensor shows a steeper slope (m = 0.0345) during this duration as compared to the PCB sensor which has a more gradual slope (m = 0.0075). As the seeding density was set to be the same for both sensors, this indicates that SiHa cells on the PET have a faster growth rate than in the PCB. This was expected from the higher gelatin yield and cell attachment observed on the PET sensor earlier.

When compared with the cell counting (Trypan blue) curve, the impedance cell growth curves show that the cells have entered exponential growth or log phase.[78] During this phase, cells actively proliferate, leading to an exponential increase in cell density.[78] The PET sensor's cell index reflects this with a sigmoid curve similar to the Trypan blue results. On the contrary, the PCB sensor exhibits a prolonged lag phase possibly due to the lower initial cell density achieved during attachment.[80]

As shown in Fig. 7d, at 72 h, both sensors have different slopes. Although both sensors still showed an increase in cell index compared to the previous data timepoint, however, the PET sensor's slope (m = 0.0029) went from gradually increasing to almost plateauing at this point. In contrast, the PCB sensor shows a consistently increasing slope (m = 0.009). from the previous time.

Table II. Comparison of SiHa cell growth phase using cell index measurements. The duration of cell growth phases was only estimated based on the graph pattern and time from the control cell index in the results of each work.

Sensor	SiHa cell seeding density	Cell Index Range	Lag Phase (hours)	Log Phase (hours)	Stationary Phase (hours)	Death Phase (hours)	References
xCELLigence	6000 cells/well	0–4.0	0–5	5–60	60–120	—	83
xCELLigence	10,000 cells/well	0–1.5	0–24	24–72	—	—	82
xCELLigence	100, 000 cells/ml	0–3.0	0–5	5–50	50–65	65–76	84
PET	50,000 cells/well	0–1.5	0–24	24–72	—	72–96	This work
PCB	50,000 cells/well	0–1.0	0–48	48–96	—	—	This work

Trypan blue cell counting and CI of the PET sensor both shows the maximum peak at 72 h. This observation suggests that the cells on the PET sensor had reached the stationary phase, where the cell proliferation slows down and there is a balance between cell growth and death rates, resulting in a plateau in cell number.[78] In contrast, the PCB sensor remained in the prolonged lag phase during this time.

At 96 h, the PET sensor displayed a decrease in cell index (m = −0.0081), suggesting the onset of the death phase, which is further supported by the declining trend observed in the cell counting data. This decrease in cell index likely reflects cell detachment from the electrode surface.[77] On the contrary, the PCB sensor (m = 0.011) continuously has an increased cell index showing that the cells have not reached confluency on the sensor yet. This observation shows that PET has better comparison in trend with the cell counting compared to the PCB sensor.

The comparisons of the two types of sensors revealed that the PET sensor achieved a higher cell index at an earlier time (48 h) compared to the PCB sensor (96 h). Although both sensors have shown compatibility with cell culture, however, there is a difference in the pattern of the cell growth curve. Cell growth in PET sensor shows a typical standard curve of all phases of cell growth; lag phase (in the first 24 h), log phase (until 48 h), stationary phase (in between 48 to 72 h), and death phase (after 72 h) almost similar to the growth pattern in cell counting method. PCB sensor shows the observation of only two phases; lag phase (in the first 48 h) and log phase (at the end of the experiment at 96 h). From the growth curve in both sensors, a prolonged log phase can be seen in the PCB sensor. An assumption can be made that the cells took a longer time to adapt to the new environment, especially on the new substrate fiberglass coated with epoxy resin which may trigger cellular stress. Cellular stress was found to be a factor that can prolong the lag phase and cause a low rate of exponential growth.[81] Further studies are required to verify the presence of cellular stress.

Experiments were conducted for up to 96 h to avoid any distortion in the impedance reading due to the presence of an edge effect in the well of the sensors. The doubling time of SiHa cells was calculated to be 28 h for the PET sensor and 51 h for the PCB sensor as shown in (Fig. 6d). This shows that the PET sensor has almost similar doubling time compared to the conventional cell counting method which was at approximately 48 h. Therefore, the PET sensor exhibits better performance compared to the PCB sensor.

To confirm the cell growth on the sensors, we examined both sensors under the microscope at the end of the experiments to detect any presence of cells on the sensors. (Figs. 7e and 7f) shows the cell growth on the PCB and PET sensors respectively. The advantage of PET is that it is a transparent substrate, and imaging can be done using a standard inverted microscope. In this experiment, SiHa cells on PET reach confluency at 96 h. This is supported by the cell index reading (specify the value) that suggests the cells are at the beginning of the death phase. In contrast, the PCB sensor has an opaque substrate, it was observed under an upright microscope with objectives placed above the sample. This type of microscope is rarely used in cellular imaging since adherent-type cells usually sink, attach, and form a monolayer at the bottom of the well. Thus, fuzzy images of cells were often produced based on our experience when

imaging live cells on electrodes. Based on (Fig. 6e), the epithelial morphology of SiHa cells was discovered to be practically circular-like in shape due to fuzzy details of the cell morphology while imaging on an opaque substrate. This provides an insight into how the cell morphology was seen under the different microscopes and based on the figure, cells were proven to grow on both sensors.

To validate the performance of the PCB and PET sensors, comparisons were made with other works that involved SiHa cell growth monitored using commercialized xCELLigence RTCA system[82–84] as shown in Table II. From the table, the maximum cell index obtained from PCB and PET sensors are slightly lower than the xCELLigence system. The cell growth phases of PET sensor are comparable to one of the works[82] where the lag phase occurred in the first 24 h of culture and log phase at 24–72 h. However, the seeding density is higher in this work therefore suggesting that the performance of the sensor could potentially be improved by increasing the surface hydrophilicity[85] and optimizing the attachment factor such as ECM and seeding cell density.

Conclusions

We have successfully characterized both Au-plated sensor materials physically and biologically. The electroplated process in the PCB sensor yields a thicker layer of Au compared to the electroless gold in PET. SEM revealed the electroplated surface to be smoother but wavier than the electroless surface which has a fine grain-like surface morphology. As for biological characterization, both sensors were concluded to be biocompatible and suitable for monitoring the growth of SiHa cells. This shows that the sensors are suitable to be used in cancer cell applications, including diagnosis, personalized treatment, drug discovery and development. PET sensors are shown to have better performance in terms of having a higher cell index and exhibit a similar trend to the conventional method as compared to the PCB sensor. However, PCB sensors have higher electrochemical migration voltage tolerance compared to the PET sensor indicating that the thickness of the metallization layer plays an important role in the electrochemical migration effect. This project hopes to encourage more use of LoP as a cell-based biosensor, especially towards point-of-care sensor applications.

ORCID

Ahmad Fairuzabadi Mohd Mansor https://orcid.org/0000-0002-2639-1703
Anis Nurashikin Nordin https://orcid.org/0000-0002-8301-4365

References

1. R. Pradhan, A. Mitra, and S. Das, *Electroanalysis*, **24**, 2405 (2012).
2. X. Zhang et al., *Sens Actuators B Chem*, **247**, 780 (2017).

3. T. Schmiedinger et al., *Biomed. Microdevices*, **22**, 1 (2020).
4. D. Mondal and C. RoyChaudhuri, *ISSS J Micro Smart Syst*, **7**, 107 (2018).
5. S-P. Chiu et al., *Sensors*, **19**, 3210 (2019).
6. L. D. Robilliard et al., *Biosensors (Basel)*, **11**, 498 (2021).
7. S. Lieb et al., *Pharmacol. Res.*, **108**, 65 (2016).
8. M. A. Nahid, C. E. Campbell, K. S. K. Fong, J. C. Barnhill, and M. A. Washington, *J. Microbiol. Methods*, **169**, 105833 (2020).
9. Y. Liang et al., *Anal. Biochem.*, **622**, 114155 (2021).
10. M. L. Gelsinger, L. L. Tupper, and D. S. Matteson, *Int J Biostat*, **16**, 20180083 (2020).
11. N. I. Ramli, N. A. B. Ismail, F. Abd-Wahab, and W. W. A. W. Salim, *in Transparent Conducting Films*, ed. K Pal (IntechOpen, London) (2018).
12. H. S. Magar, R. Y. A. Hassan, and A. Mulchandani, *Sensors*, **21**, 6578 (2021).
13. P. Ramiah Rajasekaran et al., *Microsyst. Nanoeng.*, **6**, 100 (2020).
14. M. Bielfeldt et al., *J Biol Eng*, **17**, 71 (2023), /pmc/articles/PMC10668359/.
15. Q. Liu et al., *Chem. Rev.*, **114**, 6423 (2014).
16. S. Singh, J. Wang, and S. Cinti, *ECS Sensors Plus*, **1**, 023401 (2022).
17. A. M. Mamaril, D. L. Glasco, F. A. Leal Yepes, and J. G. Bell, *ECS Sensors Plus*, **1**, 040601 (2022).
18. M. Liang et al., *ECS Sensors Plus*, **2**, 030604 (2023).
19. D. Moschou and A. Tserepi, *Lab Chip*, **17**, 1388 (2017).
20. F. Perdigones, *Micromachines (Basel)*, **12**, 175 (2021).
21. P. Jolly, J. Rainbow, A. Regoutz, P. Estrela, and D. Moschou, *Biosens. Bioelectron.*, **123**, 244 (2019).
22. G. D. Kaprou, V. Papadopoulos, C-M. Loukas, G. Kokkoris, and A. Tserepi, *Micromachines (Basel)*, **11**, 258 (2020).
23. J. D. Urbano-Gámez, F. Perdigones, and J. M. Quero, *Micromachines (Basel)*, **12**, 1071 (2021).
24. S. Anastasova, P. Kassanos, and G-Z. Yang, *Biosens. Bioelectron.*, **102**, 668 (2018).
25. H. Shamkhalichenar, C. J. Bueche, and J. W. Choi, *Biosensors (Basel)*, **10**, 159 (2020).
26. P. Zhang, S. Xue, and J. Wang, *Mater. Des.*, **192**, 108726 (2020).
27. K-N. Tu, *J. Appl. Phys.*, **94**, 5451 (2003).
28. P. Yi, K. Xiao, K. Ding, C. Dong, and X. Li, *Materials*, **10**, 137 (2017).
29. B. Medgyes, *J. Mater. Sci., Mater. Electron.*, **28**, 18578 (2017).
30. T. Braun et al., *2009 59th Electronic Components and Technology Conference* (IEEE) 1065 (2009).
31. M. Mazzuferi et al., *Biomaterials*, **31**, 1045 (2010).
32. J. D. Urbano-Gámez et al., *Micromachines (Basel)*, **12**, 1469 (2021).
33. M. Rabbani, E. Rahman, A. Al Aishan, M. B. Powner, and I. F. Triantis, *Applied Sciences (Switzerland)*, **14**, 162 (2024).
34. B. Senevirathna et al., *Biosens. Bioelectron.*, **142**, 111501 (2019).
35. A. F. M. Mansor and A. N. Nordin, *2018 7th International Conference on Computer and Communication Engineering (ICCCE)* (IEEE) 62 (2018).
36. E. Bumiller and C. Hillman, *DfR Solutions* (2009).
37. A. Ojstršek et al., *Sensors*, **21**, 3508 (2021).
38. M. T. Mubarak, I. Ozsahin, and D. U. Ozsahin, *2019 Advances in Science and Engineering Technology International Conferences (ASET)* (IEEE) 1 (2019).
39. R. Ambat and K. Piotrowska, *Humidity and Electronics: Corrosion Reliability Issues and Preventive Measures*, ed. R. Ambat (Elsevier, Netherlands) (2021).
40. X. Liu et al., *Regul. Toxicol. Pharm.*, **97**, 24 (2018).
41. V. Stock et al., *Toxicol. in Vitro*, **70**, 105021 (2021).
42. U. Kasiviswanathan et al., *J Anal Sci Technol*, **11**, 1–12 (2020).
43. A. F. M. Mansor, I. Ibrahim, A. A. Zainuddin, I. Voiculescu, and A. N. Nordin, *Med. Biol. Eng. Comput.*, **56**, 173 (2018).
44. I. Ibrahim, A. Nurashikin Nordin, Y. Zuhanis, and H-Y. Hashim, *J Pure and Appl Microbiology*, **8**, 827 (2014).
45. A. F. M. Mansor, A. N. Nordin, and I. Ibrahim, *2015 International Conference on Smart Sensors and Application (ICSSA)*, Piscataway, NJ (IEEE) 1 (2015).
46. S. Abasi, J. R. Aggas, G. G. Garayar-Leyva, B. K. Walther, and A. Guiseppi-Elie, *ACS Measurement Science Au*, **2**, 495 (2022).
47. R. Szulcek, H. J. Bogaard, and G. P. van Nieuw Amerongen, *Journal of Visualized Experiments*, **85**, 1 (2014).
48. G. Rinaldi, A. Loukas, P. J. Brindley, J. T. Irelan, and M. J. Smout, *Int J Parasitol Drugs Drug Resist*, **5**, 141 (2015).
49. M. A. U. Khalid et al., *Biochem. Eng. J.*, **155**, 107469 (2020).
50. N. Ke, X. Wang, X. Xu, and Y. A. Abassi, *Mammalian Cell Viability: Methods and Protocols*, **740**, 33 (2011).
51. M. A. Mohd Asri, W. C. Mak, S. A. Norazman, and A. N. Nordin, *Lab Chip*, **22**, 1779 (2022).
52. H. A. Barnes, *J Nonnewton Fluid Mech*, **70**, 1 (1997).
53. H. Li, S. Liu, and L. Lin, *Int J Bioprint*, **2**, 28 (2016).
54. A. Denchai, D. Tartarini, and E. Mele, *Front. Bioeng. Biotechnol.*, **6**, 155 (2018).
55. P. Panjan, V. Virtanen, and A. M. Sesay, *Talanta*, **170**, 331 (2017).
56. B. Vural, M. Çalişkan, and M. K. SezgiNtürk, *Turk. J. Chem.*, **44**, 461 (2020).
57. P. Yu and S. Dong, *Proceedings of the International Solid-State Sensors and Actuators Conference - TRANSDUCERS '95* (1995).
58. P. Wei et al., *Sensors (Switzerland)*, **18**, 59 (2018).
59. Y. Khan et al., *Adv. Mater.*, **32**, 1905279 (2020).
60. M. Lé-Magda et al., *Macromol. Symp.*, **315**, 143 (2012).
61. L. Frisk, S. Lahokallio, J. Kiilunen, and K. Saarinen-Pulli, *MRS Adv.*, **1**, 3477 (2016).
62. C. Xie, X. Tang, B. Song, and J. Jin, *Proceedings of the 2012 2nd International Conference on Instrumentation and Measurement, Computer, Communication and Control, IMCCC 2012*1661 (2012).
63. B. I. Noh and S. B. Jung, *J. Mater. Sci., Mater. Electron.*, **19**, 952 (2008).
64. J. A. Jachim, G. B. Freeman, and L. J. Turbini, *IEEE Transactions on Components, Packaging, and Manufacturing Technology: Part B*, **20**, 443 (1997).
65. M. J. Gira, K. P. Tkacz, and J. R. Hampton, *Nano Converg*, **3**, 6 (2016).
66. N. Elgrishi et al., *J. Chem. Educ.*, **95**, 197 (2018).
67. T. Pajkossy, *Electrochim. Acta*, **308**, 410 (2019).
68. M. A. A. M. Asri, W. C. Mak, S. A. Norazman, and A. N. Nordin, *Lab Chip*, **22**, 1779 (2022).
69. J. A. Hondred, Z. T. Johnson, and J. C. Claussen, *J Mater Chem C Mater*, **8**, 11376 (2020).
70. M. S. F. Santos, W. A. Ameku, I. G. R. Gutz, and T. R. L. C. Paixão, *Talanta*, **179**, 507 (2018).
71. D. Evans et al., *Sensors (Switzerland)*, **18**, 4011 (2018).
72. B. D. Matthews, D. R. Overby, R. Mannix, and D. E. Ingber, *J. Cell Sci.*, **119**, 508 (2006).
73. C. Zhu, G. Bao, and N. Wang, *Annual Rev. of Biomed. Eng.*, **2**, 189 (2000).
74. F. Boccafoschi, M. Bosetti, P. M. Sandra, M. Leigheb, and M. Cannas, *Cell Adh Migr*, **4**, 19 (2010).
75. J. A. Espina, M. H. Cordeiro, M. Milivojevic, I. Pajić-Lijaković, and E. H. Barriga, *J. Cell Sci.*, **136**, 1 (2023).
76. J. C. Gil-Redondo, A. Weber, M. dM. Vivanco, and J. L. Toca-Herrera, *Microsc. Res. Tech.*, **86**, 1069 (2023).
77. R. Ehret et al., *Biosens. Bioelectron.*, **12**, 29 (1997).
78. J. E. Celis, *Cell Biology: a Laboratory Handbook* (Elsevier, Amsterdam) (2006).
79. J. A. DeQuach et al., *PLoS One*, **5**, e13039 (2010).
80. R. L. Bertranda, *J. Bacteriol.*, **201**, 7 (2019).
81. P. G. Hamill et al., *Sci Rep*, **10**, 1 (2020).
82. C. Liu et al., *Transl. Cancer Res.*, **11**, 1089 (2022).
83. P. Khumkhrong et al., *Biomolecules*, **9**, 494 (2019).
84. V. A. Mitkevich et al., *Oncotargets*, **8**, 72666 (2017).
85. C. H. Kim, M. S. Khil, H. Y. Kim, H. U. Lee, and K. Y. Jahng, *J Biomed Mater Res B Appl Biomater*, **78B**, 283 (2006).
86. C. Franck, S. A. Maskarinec, D. A. Tirrell, and G. Ravichandran, *PLoS One*, **6**, e17833 (2011).